The Astrophysical Journal Supplement Series, 220:13 (11pp), 2015 September doi:10.1088/0067-0049/220/1/13

IMPROVED Co I log(*gf*) VALUES AND ABUNDANCE DETERMINATIONS IN THE PHOTOSPHERES OF THE SUN AND METAL-POOR STAR HD 84937

J. E. Lawler[1], C. Sneden[2], and J. J. Cowan[3]
[1] Department of Physics, University of Wisconsin-Madison, 1150 University Ave., Madison, WI 53706, USA; jelawler@wisc.edu
[2] Department of Astronomy and McDonald Observatory, University of Texas, Austin, TX 78712, USA; chris@verdi.as.utexas.edu
[3] Homer L. Dodge Department of Physics and Astronomy, University of Oklahoma, Norman, OK 73019, USA; jjcowan1@ou.edu
Received 2015 June 4; accepted 2015 July 28; published 2015 September 11

ABSTRACT

New emission branching fraction measurements for 898 lines of the first spectrum of cobalt (Co I) are determined from hollow cathode lamp spectra recorded with the National Solar Observatory 1 m Fourier transform spectrometer on Kitt Peak, AZ and a high-resolution echelle spectrometer. Published radiative lifetimes from laser induced fluorescence measurements are combined with the branching fractions to determine accurate absolute atomic transition probabilities for the 898 lines. Hyperfine structure (hfs) constants for levels of neutral Co in the literature are surveyed and selected values are used to generate complete hfs component patterns for 195 transitions of Co I. These new laboratory data are applied to determine the Co abundance in the Sun and metal-poor star HD 84937, yielding $\log \varepsilon(\mathrm{Co}) = 4.955 \pm 0.007$ ($\sigma = 0.059$) based on 82 Co I lines and $\log \varepsilon(\mathrm{Co}) = 2.785 \pm 0.008$ ($\sigma = 0.065$) based on 66 Co I lines, respectively. A Saha or ionization balance test on the photosphere of HD 84937 is performed using 16 UV lines of Co II, and good agreement is found with the Co I result in this metal-poor ([Fe I/H] = −2.32, [Fe II/H] = −2.32) dwarf star. The resulting value of [Co/Fe] = +0.14 supports a rise of Co/Fe at low metallicity that has been suggested in other studies.

Key words: atomic data – stars: individual (HD 84937) – stars: Population II – Sun: abundances

Supporting material: machine-readable tables

1. INTRODUCTION

The production of iron- (Fe-) group elements in early supernovae (SNe) is known to yield relative abundance values significantly different from the relative Solar values of those elements (e.g., Henry et al. 2010). The increasing role of Type Ia SNe as the Galaxy aged explains only part of the anomalous abundance trends, which for the Fe-group can cover ±1 dex for metallicities ranging from solar ([Fe/H] ≡ 0) to −4 (e.g., Figure 12 of McWilliam 1997).[4]

Interest in early nucleosynthesis and the Galactic chemical evolution is high. Modeling of events now being observed as gamma-ray bursts (GRBs) is revealing some details of early nucleosynthesis. Long GRBs at the highest red shifts are now thought to be early core collapse SNe, likely from very massive stars at (near-) zero metallicity, and perhaps rapidly rotating. Short GRBs at somewhat lower red shifts are now thought to be *n*(eutron)-star plus *n*-star or black hole mergers. Elemental abundance studies on metal-poor stars provide important constraints on the modeling.

Our collaboration is working through the Fe-group neutral or first (e.g., Co I) and singly ionized or second (e.g., Co II) spectra with the long term goals of improving laboratory data for Fe-group elements using the best available experimental techniques and applying such data to explore the limits of standard one-dimensional/local thermal equilibrium (1D/LTE) photospheric models (Asplund 2005 discusses the need for 3D/non-LTE; NLTE models). Possible departures from Saha balance are of particular interest because they are thought to be the dominant NLTE effect in most stellar photospheres. The long-term objective of our studies is to map the relative abundances of Fe-group elements at low metallicity. This paper complements the very recent studies on V I (Lawler et al. 2014) and V II (Wood et al. 2014a) and recent work on other spectra including Cr I (Sobeck et al. 2007), Mn I and Mn II (Den Hartog et al. 2011), Ti I (Lawler et al. 2013), Ti II (Wood et al. 2013), Ni I (Wood et al. 2014b), and Fe I (Den Hartog et al. 2014; Ruffoni et al. 2014). Our new transition probability data are supplemented with improved isotopic and hyperfine structure (hfs) data as needed. As a first application of these Fe-group data, we determine improved elemental abundances in the Sun and metal-poor turnoff star HD 84937.

This paper reports new emission branching fractions and absolute atomic transition probability measurements for 898 lines of Co I, complete hfs line component patterns for 195 lines of Co I that are useful in abundance studies, a new solar abundance determination of $\log \varepsilon(\mathrm{Co}) = 4.955 \pm 0.007$ ($\sigma = 0.059$), where σ is the standard deviation of the abundance based on 82 Co I lines, and a new abundance determination in HD 84937 of $\log \varepsilon(\mathrm{Co}) = 2.785 \pm 0.008$ ($\sigma = 0.065$) based on 66 Co I lines using the Holweger-Müller (1974) 1D model. The hfs line component patterns for 195 transitions are based on published hfs coefficients. The new transition probabilities are put on a highly reliable absolute scale using radiative lifetimes from laser induced fluorescence (LIF) measurements (Nitz et al. 1995) of the upper levels for all 898 transitions. Machine-readable tables for both the transition probability and hfs line component patterns are provided to support continuing studies of metal-poor stars.

2. BRANCHING FRACTION MEASUREMENTS FOR LINES OF CO I

Data from two complementary spectrometers are used in this work on Co I including both the 1 m Fourier transform

[4] We use standard abundance notations. For elements X and Y, the relative abundances are written $[\mathrm{X/Y}] = \log10(N_\mathrm{X}/N_\mathrm{Y})_\mathrm{star} - \log10(N_\mathrm{X}/N_\mathrm{Y})_\mathrm{Sun}$. For element X, the "absolute" abundance is written $\log \varepsilon(\mathrm{X}) = \log_{10}(N_\mathrm{X}/N_\mathrm{H}) + 12$. Metallicity is defined as [Fe/H].

spectrometer (FTS) at the National Solar Observatory (NSO) and a 3 m focal length echelle spectrometer. More information on these instruments is in our recent work on V I (Lawler et al. 2014) and V II (Wood et al. 2014a). The FTS, which provides better wave number measurements, is described by Brault (1976) and the echelle spectrometer, which is free from multiplex noise, is described by Wood & Lawler (2012).

Table 1 lists the 17 spectra from the NSO 1 m FTS.[5] Table 2 lists the spectra from the 3 m echelle spectrometer used in this Co I study. Spectra in both lists are from low-pressure hollow cathode lamps, which yield very narrow lines from sputtered metal. The use of spectra covering a range of lamp current and two or more buffer gases enables one to avoid optical depth errors and to separate many blended lines.

Branching fraction measurements are not attempted for all 135 levels of neutral cobalt with radiative lifetimes measured by Nitz et al. (1995) due to branches below 2000 Å from some upper levels. Although the 3 m echelle is a vacuum instrument by design, the order separator is not yet vacuum compatible. Branching fractions are completed for 101 levels total including 99 odd parity levels and 2 even parity levels. Improved energy levels from Pickering & Thorne (1996) are used to evaluate the wavenumber of every possible transition satisfying the parity change and $|\Delta J| \leqslant 1$ selection rules from the upper levels of interest. Analysis of the data is discussed in more detail in earlier papers (e.g., Lawler et al. 2014).

Our usual technique for separating ion/neutral line blends exploits the current dependence of the total integrated feature (e.g., Lawler et al. 2011) and is used on about six Co I plus Co II line blends. Blends of pairs of Co I lines often have almost no current dependence but are separable in FTS data using the accurate energy levels reported by Pickering & Thorne (1996). This center-of-gravity (cog) separation method is also applicable to Co I and Co II line blends using the accurate energy levels of Co II by Pickering et al. (1998). A comparison of the cog of the blended feature to Ritz wavenumbers for both contributing transitions and a requirement that a normalized and weighted combination of the Ritz wavenumbers match the cog of the blended feature yields the fractional contribution of each line. A high signal-to-noise ratio (S/N) is needed as well as separation of 0.05 cm^{-1} or more.

A relative radiometric calibration is essential to convert the above transition strengths from numerical integration into strengths proportional to photons per unit time. The Ar I and Ar II branching ratios established and checked by Adams & Whaling (1981), Danzmann & Kock (1982), Hashiguchi & Hasikuni (1985), and Whaling et al. (1993) are used to calibrate FTS data. The relative radiometric calibration of the echelle spectrometer is from National Institute of Standards and Technology (NIST) traceable D_2 lamp spectra recorded immediately after each hollow cathode CCD frame. More detail is available in recent work on V I (Lawler et al. 2014). Our heavily used D_2 lamp is periodically checked against another NIST-traceable D_2 lamp that has far fewer hours of operation, and against a windowless Ar miniarc (Bridges & Ott 1977) calibrated personally by Dr. Bridges at NIST. The echelle data on Co I are primarily used in the UV to provide better sensitivity, test for optical depth errors, and test the UV calibration of the FTS data.

Sometimes a correction for "residuals" or unobserved lines is performed in branching fraction studies. No correction is applied to our branching fractions. The high current FTS data in Table 1 enabled us to measure weak branches in the UV, optical and near-IR. Most of the radiative lifetimes of neutral Co are sufficiently short, <100 ns, to alleviate concerns about longer wavelength IR residuals.

Uncertainties on final average branching fractions are evaluated using the strength of the branching fraction, the S/N of the data, and the wavenumber separation of lines from the common upper level. Uncertainty always migrates to the weaker branches. The calibration uncertainty is estimated to be 0.001%/cm^{-1} of separation between a line and the dominant branch(es) from the common upper level (Wickliffe et al. 2000). This calibration uncertainty is combined with the standard deviation of results from multiple spectra and the above factors to determine the branching fraction uncertainty.

3. CO I TRANSITION PROBABILITIES FOR 898 LINES AND COMPARISON TO EARLIER MEASUREMENTS

Transition probabilities are given in Table 3 for 898 lines of Co I. Lifetimes from Nitz et al. (1995) are used to establish the absolute scale and convert the emission branching fractions described in the preceding section into accurate absolute Einstein *A* coefficients. Energy levels are from Pickering & Thorne (1996) and wavelengths are computed using Ritz wavenumbers and the standard refractive index of air (Peck & Reeder 1972). The sums of the transition probabilities for lines connected to some upper levels are less than the inverse of the upper level lifetimes, typically by a few percent, due to weak transitions that have been omitted from Table 3 but kept in the branching fraction normalization. Such weak lines are omitted due to ambiguous or dual classifications, blending, or poor S/N, but these omitted weak branches have little effect on the transition probabilities in Table 3 and almost no effect on the transition probability uncertainties in Table 3.

An important set of comparisons between our Co I atomic transition probability measurements and earlier work is based on the online NIST Atomic Spectra Database[6] (ASD; Kramida et al. 2014). A search of the NIST ASD for Co I lines with transition probabilities in the ASD and in Table 3 yields 105 lines for comparison. All of these transition probabilities are originally from Cardon et al. (1982). These authors used both hook measurements and emission branching fractions normalized with radiative lifetimes from LIF measurements (Figger et al. 1975; Marek & Vogt 1977). A few of their spectra from the NSO 1 m FTS may also be included in Table 1, but our comparison treats their data set as independent with NIST ASD uncertainties combined in quadrature with our uncertainties in Figures 1(a) and (b). There is no overlap of lifetime data and the FTS spectral analysis was independent. The NIST ASD uncertainties ranged from *B* (±10% or better) to *D* (±50% or better) with mostly *C* (±25% or better) and *C*+ which we treated as *C*.

The outlier at 2530.135 Å attracts one's attention. Pickering & Thorne (1996) classified the line from the upper level at 44201.849 cm^{-1} to the lower level at 4690.141 cm^{-1} and indicated it is strong based on its S/N in their spectra. In the NIST ASD the lower level is pure $3d^8(^3F)4\,s\,^4F\,J = 5/2$ and the upper level is also $J = 5/2$ with 29% $3d^7(^2G)4s4p(^3P)\ ^4F$.

[5] FTS data are publicly available at http://diglib.nso.edu/.

[6] http://physics.nist.gov/PhysRefData/ASD/lines_form.html

Table 1

Fourier Transform Spectra of Commercial Sealed Hollow Cathode Discharge (HCD) Lamps at Low Current (<100 mÅ) and of Custom Water-cooled HCD Lamps at High Current (>100 mÅ)

Index	Date	Serial Number	Buffer Gas	Lamp Current (mÅ)	Wavenumber Range (cm^{-1})	Limit of Resolution (cm^{-1})	Coadds	Beam Splitter	Filter	Detector[a]
1	1982 Aug 14	5	Ar–Ne	600	7375–49105	0.057	8	UV	none	Large UV Si Diode
2	1979 Dec 11	3	Ar	300	7454–44367	0.058	11	UV	CS9-54	Super Blue Si Diode
3	1983 Nov 14	6	Ar–Ne	600	14492–40610	0.047	54	UV	CuSO4	Large UV Si Diode
4	1979 Dec 13	4	Ar	315	14607–37023	0.047	8	UV	CuSO4 + CS9-54	Si Diode
5	1979 Mar 12	2	Ar	230	6967–31851	0.061	8	Vis	CS7-59 + CS4-97 + WG345	Mid Range Si Diode
6	1979 Mar 13	3	Ar	150	10732–28921	0.055	8	Vis	CS4-97 + GG375 + TC	Mid Range Si Diode
7	1978 Sep 11	2	Ar	150	7682–28921	0.055	8	Vis	GG375 + TC	Super Blue Si Diode
8	1978 Sep 11	5	Ar	150	14912–28920	0.055	8	UV	CS 4-96 + WG375 + TC	Super Blue Si Diode
9	1978 Sep 12	8	Ar	⋯	7658–19034	0.036	8	Vis	OOG570	Super Blue Si Diode
10	1979 Mar 13	4	Ar	150	7584–18439	0.036	10	Vis	OG570	Super Blue Si Diode
11	1978 Sep 12	5	Ar	160	3262–12103	0.023	8	Vis	Ga-As	Super Blue Si Diode
12	1997 Dec 20	1	Ar	24	7929–34998	0.053	4	UV	none	Super Blue Si Diodes
13	1997 Dec 20	2	Ar	17.5	7929–34998	0.053	4	UV	none	Super Blue Si Diodes
14	1997 Dec 20	3	Ar	11	7929–34998	0.053	4	UV	none	Super Blue Si Diodes
15	1982 Aug 14	2	Ne	600	7883–44074	0.053	8	UV	none	Large UV Si Diode
16	1982 Aug 14	3	Ne	600	8198–24691	0.029	8	UV	GG435	Large UV Si Diode
17	1982 Aug 14	4	Ne	600	2553–11725	0.014	8	UV	GaAs	InSb

Notes. All spectra were recorded using the 1 m FTS on the McMath Telescope at the National Solar Observatory, Kitt Peak, AZ.

[a] Detector types include the Super Blue silicon (Si) photodiode, Large UV Si photodiode, Mid Range Si photodiode, and InSb detectors for the IR. The UV beam splitter is fused silica.

Table 2
Echelle Spectra of Sealed Commercial HCD Lamps

Index	Date	Serial Numbers[a]	Buffer Gas	Lamp Current (mÅ)	Wavelength Range (Å)	Resolving Power	Coadds	Exposure Time (s)
31–35	2014 Aug 8	1, 3, 5, 7, 9	Ar	10	2100–3200	250,000	27	200
36–40	2014 Aug 19	1, 3, 5, 7, 9	Ar	10	2100–3200	250,000	60	88
41–45	2014 Aug 20	1, 3, 5, 7, 9	Ne	15	2100–3200	250,000	180	30
46–50	2014 Aug 22	1, 3, 5, 7, 9	Ne	20	2100–3200	250,000	540	10
51–55	2015 Jan 17	1, 3, 5, 7, 9	Ar	10	2200–3900	250,000	27	200
56–60	2015 Jan 19	1, 3, 5, 7, 9	Ar	15	2200–3900	250,000	60	90
61–65	2015 Jan 15	1, 3, 5, 7, 9	Ne	15	2200–3900	250,000	300	18
66–70	2015 Jan 16	1, 3, 5, 7, 9	Ne	20	2200–3900	250,000	540	10

Note.
[a] At least 3 CCD frames are needed to capture a complete echelle grating order in the UV. In the above data 5 CCD frames are used to provide redundancy and a check for lamp drift.

Table 3
Experimental Atomic Transition Probabilities for 898 Lines of Co I Organized by Increasing Wavelength in Air

Wavelength in Air	Upper Level			Lower Level			Transition Probability	log(*gf*)
(Å)	Energy[b] (cm^{-1})	Parity	*J*	Energy[b] (cm^{-1})	Parity	*J*	(10^6 s^{-1})	
2073.2847	48217.260	od	3.5	0.000	ev	4.5	3.2 ± 0.5	−1.78
2082.1148	48828.801	od	2.5	816.000	ev	3.5	0.60 ± 0.05	−2.63
2098.9514	48443.716	od	2.5	816.000	ev	3.5	8.0 ± 1.2	−1.50
2111.4057	48753.666	od	1.5	1406.852	ev	2.5	1.88 ± 0.29	−2.30
2116.8514	47225.026	od	3.5	0.000	ev	4.5	1.79 ± 0.20	−2.02

Notes.
[a] Wavelength values computed from energy levels using the standard index of air from Peck & Reeder (1972).
[b] Energy levels are from Pickering & Thorne (1996).

(This table is available in its entirety in machine-readable form.)

Pickering & Thorne reassigned the upper level as $3d^7(^2G)4s4p$ (^3P) w^4F^o. We checked the wavenumber of the line in our FTS data and found agreement with the Ritz value and new classification. The branching fraction was measured on both Ar/Co and Ne/Co HCD lamp spectra to eliminate any possibility of a buffer gas blend. We think the line is correctly classified and that our transition probability is in Table 3 is correct.

Since the last update of the NIST ASD, the most significant work on transition probabilities of Co I was by Nitz et al. (1999) at Saint Olaf College using spectra from the NSO 1 m FTS. Nitz et al. (1999) used the Nitz et al. (1995) lifetimes to normalize their transition probabilities for 103 lines of Co I. (The lifetime measurements were performed while Prof. Nitz was on sabbatical using the LIF experiment at the Univ. of Wisconsin.) Since both the lifetime data (dominant uncertainty on strong branches of ±5%) and some of the FTS data overlap our more extensive work, only uncertainties from Nitz et al. were included in the comparisons of Figures 2(a) and (b). Agreement is quite good as expected.

4. THE COBALT ABUNDANCE IN THE SOLAR PHOTOSPHERE

To derive a new Co abundance for the Sun, we follow in all respects the methods used in our studies of V I (Lawler et al. 2014) and V II (Wood et al. 2014a). Those papers; here we briefly discuss the procedures.

Relative Co I transition strengths in the Sun can be approximated by

$$\mathrm{STR} \equiv \log(gf) - \theta\chi,$$

where χ is the excitation energy in eV, and the inverse temperature $\theta = 5040/T$. This calculation is not extremely sensitive to assumed values of θ for G-K stars, so for simplicity we adopt $\theta = 1$. The $\log(gf)$ values are those of Table 3. The resulting STR values for all Co I lines are shown in Figure 3, and we add red circles to indicate lines used in our solar analysis. From preliminary inspection of Co I lines in the solar photospheric spectrum (Delbouille et al. 1973),[7] we have determined that lines with STR ≈ −4.4 produce reduced widths $\log(\mathrm{RW}) = \log(\mathrm{EW}/\lambda) \sim -6$ (corresponding to EW ≈ 5 mÅ at 5000 Å). Lines of approximately this strength or greater are promising transitions for a Co solar abundance analysis. The red-circled points of Figure 3, those that contribute to our solar abundance analysis, have strength values STR ⩾ −5, equivalent to log(RW) ⩾ −6.6 (EW ∼ 1 mÅ).

Initially we consider all 898 transitions in Table 3, but arrive at a set of about 90 potentially useful solar Co I features by eliminating those transitions that are too weak (very low STR values), or too strong (saturated, thus insensitive to abundance changes), or too blended with other atomic/molecular absorbers, or lie in the vacuum UV ($\lambda < 3000$ Å). We compute synthetic spectra for these 90 transitions with the current

[7] http://bass2000.obspm.fr/solar_spect.php

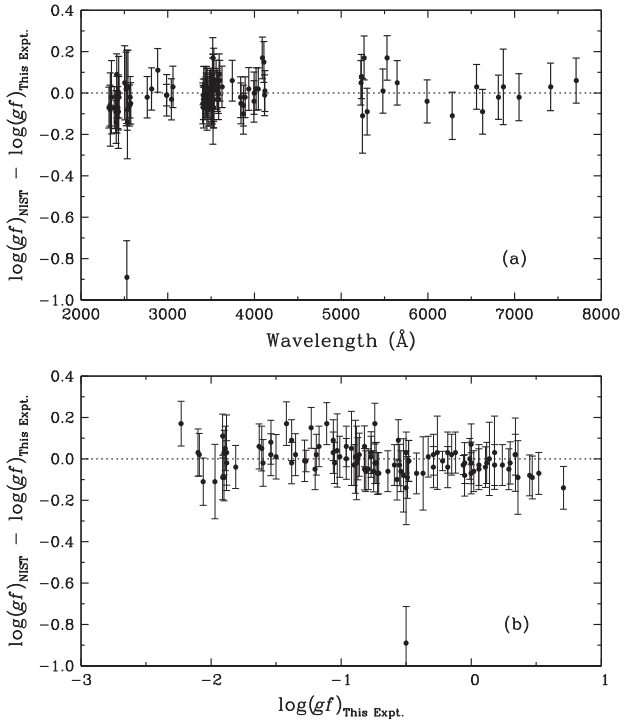

Figure 1. (a) Comparison of log(*gf*) values for 105 lines from the NIST ASD to our values as a function of wavelength. The error bars are the ASD uncertainty combined in quadrature with the uncertainty from this experiment. The central line indicates perfect agreement. The NIST ASD results are originally from Cardon et al. (1982). (b) The same except as a function of $\log(gf)_{\rm This\ Expt.}$ The outlier at 2530.135 Å is discussed in detail in the text. An upper level reassignment and line reclassification in Pickering & Thorne (1996) are correct.

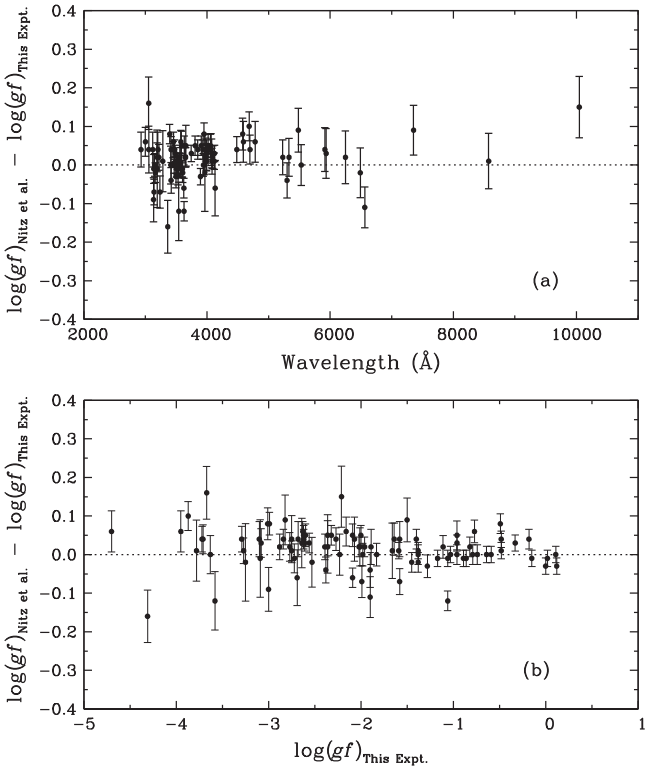

Figure 2. Comparison of log(*gf*) values for 97 lines from the Nitz et al. (1999) to our values as a function of wavelength. The error bars are from Nitz et al. only because the same set of radiative lifetimes provide the normalization of both sets of log(*gf*) values. (b) The same except as a function of $\log(gf)_{\rm This\ Expt.}$

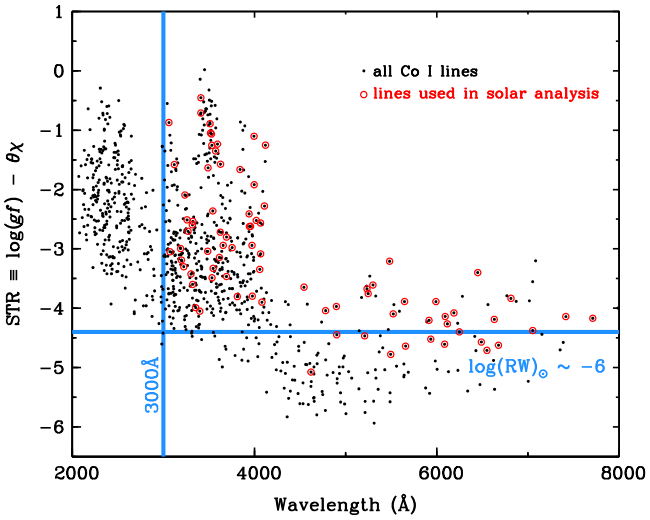

Figure 3. Relative strengths STR of Co I lines vs. wavelength; see text for discussion. A vertical blue line is drawn at the 3000 Å atmospheric cutoff. A horizontal blue line indicates the STR values of very weak lines (reduced widths log(RW) = –6). Our solar analysis includes those lines encircled here in red.

version of the LTE line analysis code MOOG[8] (Sneden 1973). Line list assembly is described in detail by Lawler et al. (2013). Synthetic spectra computed using MOOG with the Holweger & Müller (1974) solar model photosphere are then convolved with a Gaussian to empirically match the instrument profile and solar macroturbulence, and finally compared to the Delbouille et al. (1973) solar spectrum. Comparisons of observed and synthetic solar spectra force elimination of some of the Co I candidate lines that turn out to be too blended or too weak for reliable analysis. Of the 898 lines with new log(*gf*) values given in Table 3, only 82 survive the final cut.

Derivation of accurate Co I abundances must account for the hyperfine substructures discussed in the Appendix. Broadening of the line profiles by hfs can often dominate the stellar thermal and microturbulent line widths, and can significantly desaturate the lines. Many Co I lines in the solar spectrum have wide hyperfine splitting. Laboratory hyperfine data exist for all of our chosen solar Co I transitions. Straightforward entry of these hyperfine substructures into the synthetic spectra leads to final abundance estimates for each line.

In Table 4 we give transition data and derived abundances for the 82 Co I lines. We compute a mean photospheric Co abundance $\langle \log \varepsilon \rangle = 4.955 \pm 0.007$ ($\sigma = 0.059$). This value is in agreement with that of Scott et al. (2015), whose analysis used only 11 Co I lines but included much more extensive atmospheric and line formation computions that are done here. The line abundances are plotted as functions of excitation energy and wavelength in Figure 4. There is no correlation of abundance with excitation energy χ (panel (a)). Inspection of the plot of abundance versus wavelength (panel (b)) indicates that several lines in the near-UV spectral region yield somewhat lower abundances. The mean Co abundance for $\lambda > 3600$ Å is $\langle \log \varepsilon \rangle = 4.965$ ($\sigma = 0.057$, 64 lines), while for

[8] Available at http://www.as.utexas.edu/~chris/moog.html

Table 4
Cobalt Abundances in the Solar Photosphere from Individual Co I Lines

Wavelength (Å)	χ (eV)	log(gf)	log ε
3061.820	0.101	−0.77	4.99
3073.519	1.739	−1.31	4.84
3121.418	0.000	−1.58	4.99
3189.756	0.224	−2.77	4.96
3198.661	0.629	−2.56	4.99
3237.026	0.101	−1.99	4.89
3260.819	2.041	−0.47	4.86
3271.783	1.954	−0.75	4.89
3303.880	1.784	−1.64	4.89
3319.480	2.925	0.33	4.89
3321.909	2.079	−1.52	4.92
3325.244	2.006	−0.53	4.84
3355.941	2.041	−1.95	4.99
3400.467	1.739	−2.31	4.91
3412.336	0.513	0.06	4.91
3412.633	0.000	−0.71	4.99
3487.713	1.881	−1.16	4.89
3491.318	0.224	−1.41	4.94
3513.480	0.101	−0.79	4.89
3518.348	1.048	0.00	4.89
3529.033	0.174	−0.89	4.94
3533.358	0.224	−1.03	4.99
3534.766	2.278	−1.21	4.99
3543.259	1.881	−0.48	4.84
3546.707	1.709	−1.62	4.93
3574.965	0.581	−0.77	4.99
3594.872	0.174	−1.06	4.99
3615.389	1.954	−1.19	4.87
3624.957	0.629	−2.09	4.94
3627.807	0.513	−1.06	4.99
3656.964	0.581	−2.36	4.86
3693.361	2.006	−1.46	5.14
3693.476	2.041	−0.76	4.97
3755.449	2.079	−0.90	4.99
3812.456	1.784	−2.02	5.02
3842.049	0.922	−0.74	4.99
3941.731	0.431	−1.98	4.92
3945.326	0.922	−1.70	4.99
3957.929	0.581	−2.04	4.94
3973.140	1.881	−1.06	4.84
3977.182	2.326	−1.47	4.99
3995.307	0.922	−0.18	4.97
3997.903	1.048	−0.87	4.91
4020.899	0.431	−2.09	4.99
4058.597	2.006	−1.34	5.04
4066.366	0.922	−1.64	5.09
4068.541	1.954	−1.13	4.89
4082.593	0.629	−3.27	5.02
4110.532	1.048	−1.23	5.02
4121.318	0.922	−0.33	5.02
4543.812	2.716	−0.93	4.99
4620.824	2.716	−2.36	5.04
4781.428	1.881	−2.16	4.99
4899.514	2.041	−1.93	4.94
4904.170	2.868	−1.58	4.99
5210.039	3.407	−1.06	4.89
5235.183	2.135	−1.54	5.04
5247.920	1.784	−1.97	4.98
5301.041	1.709	−1.90	4.91
5483.354	1.709	−1.50	5.00
5495.675	3.407	−1.37	5.04
5523.297	2.326	−1.77	4.99
5647.234	2.278	−1.61	4.98
5659.115	2.040	−2.60	4.94
5915.550	2.135	−2.07	4.99
5935.390	1.881	−2.64	4.92
5991.873	2.079	−1.81	4.95
6086.657	3.407	−1.20	4.99
6093.141	1.739	−2.40	5.00
6116.990	1.784	−2.48	4.95
6188.996	1.709	−2.37	5.02
6249.500	2.040	−2.36	4.90
6450.250	1.709	−1.69	4.92
6490.328	2.040	−2.53	4.92
6551.449	1.881	−2.83	4.92
6632.440	2.278	−1.91	4.91
6678.809	1.954	−2.67	5.04
6814.944	1.954	−1.88	4.95
7054.036	2.716	−1.66	4.93
7417.382	2.041	−2.10	4.94
7712.663	2.540	−1.63	4.94

Note. hfs substructure has been incorporated in all transitions listed here.

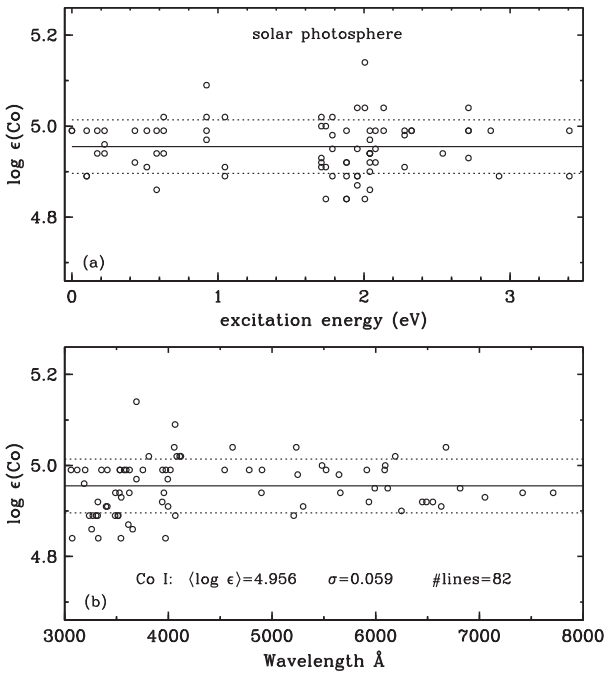

Figure 4. Cobalt abundances in the solar photosphere, plotted as functions of excitation energy χ (panel (a)) and wavelength (panel (b)). The abundance statistics appear in the bottom panel. The mean abundance is indicated with a solid line in each panel, and the 1σ deviations from the mean are shown with dotted lines.

$\lambda < 3600$ Å $\langle \log \varepsilon \rangle = 4.921$ ($\sigma = 0.053$, 18 lines). However, most of the Co I lines below 3600 Å are either very strong (saturated) in spite of their hyperfine substructure, or are blended, or are subject to very uncertain continuum placement in this crowded spectral region. Given these analytical difficulties, we do not regard this small trend with wavelength as significant.

The standard deviation of our mean abundance is only 0.007, which clearly is not a true measure of the photospheric Co

abundance uncertainty. Choice of photospheric model atmosphere and assumptions about line formation physics will dominate the Co abundance error estimate. A thorough examination of these issues has been performed by Scott et al. (2015), and will not be attempted here. They base their Co analysis partly on a previous investigation by Bergemann et al. (2010). They test several solar model atmospheres, and consider the effects of NLTE and 3D line formation calculations. Their final recommended photospheric Co abundance is $\log \varepsilon = 4.93 \pm 0.05$. From calculations involving EWs of 13 Co I lines in the yellow–red spectral region ($\lambda > 5200$ Å) and the Holweger & Müller (1974) model atmosphere, they derive $\log \varepsilon(\mathrm{Co}) = 4.94$ assuming LTE, and 4.99 with inclusion of NLTE abundance corrections. Our LTE-based abundance of $\log \varepsilon = 4.96$ is consistent with their value. Investigation of NLTE effects on our much larger set of Co I lines is beyond the scope of this paper. Considering that Scott et al. quote a range of 0.06 dex for solar Co abundances computed with different model atmospheres and line formation assumptions, we suggest a final photospheric abundance of $\langle \log \varepsilon \rangle = 4.955 \pm 0.030$.

Finally, note that our photospheric Co abundance, like that recommended by Scott et al. (2015), is somewhat larger by 0.09 dex than the meteoritic value of $\log \varepsilon = 4.87 \pm 0.01$ (Lodders et al. 2009). However, there are offsets for other Fe-group elements as well. The mean of the photospheric-meteoritic abundance differences from Table 4 of Scott et al. is $<|\log \varepsilon_{\mathrm{Sun}} - \log \varepsilon_{\mathrm{meteor}}| \geqslant 0.05$. Future investigations to reduce this scatter will be welcome.

5. THE COBALT ABUNDANCE OF METAL-POOR STAR HD 84937 FROM NEUTRAL-SPECIES TRANSITIONS

In this series of papers presenting new Fe-group transition data, we have derived abundances for both the Sun and the metal-poor main-sequence turnoff star HD 84937. We have chosen HD 84937 because its effective temperature and gravity can be determined "externally" from colors and parallax rather than the spectra under study. Only the metallicity and microturbulent velocity need to be extracted from the spectra.

In previous papers (e.g., Lawler et al. 2013) we have developed the rationale for our model parameter choices: $T_{\mathrm{eff}} = 6300$ K, $\log g = 4.0$, $[\mathrm{Fe/H}] = -2.15$, and $v_{\mathrm{t}} = 1.5$ km s^{-1}. The high temperature and gravity of this main sequence star suggest, and our calculations confirm, that H^- is the dominant continuous opacity source in nearly all spectral regions of interest for our Co abundance computations. Relative to commonly studied low metallicity red giants, in atmospheres of stars like HD 84937 collisional excitation and ionization processes are more important than radiative processes in determining Co I energy level populations.

Our search for useful Co I features in HD 84937 turned up no detectable transitions redward of 4121 Å. This is not surprising, because most of the solar features especially in the yellow–red spectral region are weak, and the metallicity of HD 84937 is more than a hundred times smaller than the Sun. The two previous general abundance studies of HD 84937 (Fulbright 2000; Gratton et al. 2003) do not report Co abundances. To our knowledge Bergemann et al. (2010) is the sole literature source, reporting a small relative overabundance: $[\mathrm{Co/Fe}] = +0.18$ from their LTE analysis and a much larger value, $[\mathrm{Co/Fe}] = +0.66$, after application of NLTE corrections. Fortunately many Co I lines are detectable in the violet and UV spectral regions of HD 84937; lines that were too strong for analysis in the Sun become prime Co abundance indicators in this star.

With the same synthetic spectrum analysis technique for Co I features that we have employed for other species in previous papers, we determine the abundances for 66 lines in HD 84937. They are listed in Table 5. To derive these abundances we employ the version of MOOG that has scattering included in the continuum source function (Sobeck et al. 2011). However for HD 84937 (and other main-sequence turnoff stars) the scattering contributions are very small; H^- is the dominant continuum opacity source, followed by H I Balmer continuum opacity in the 3100–3650 Å spectral region.

Hyperfine substructure in strong UV Co I lines is a significant issue for our HD 84937 analysis, but unfortunately we lack laboratory data for some lines of interest. Therefore we examine each potentially useful Co I line in the FTS very high-resolution emission spectrum discussed in Section 2. We first judge visually whether a line appears to be single at the resolution of the lab spectrum, that is, whether its profile seems to be symmetric and narrow. This is followed by a simple quantitative test. We measure the full width of a line at a flux level 10% above the baseline (no line emission), and convert that wavelength spread into velocity units. We find that lines with $v_{10\%} < 4$ km s^{-1} all have simple and symmetric profiles, while those with larger measured velocity widths appear to have substructure in their profiles. The stellar Doppler full width at half maximum (from the combination of thermal and microturbulent broadening) is about 4.5 km s^{-1} for HD 84937. The equivalent velocity spread closer to the stellar continuum is $v_{10\%} \geqslant 10$ km s^{-1}. Therefore for the HD 84937 abundance analysis we treat all "simple" Co I lines (those with lab $v_{10\%} < 4$ km s^{-1}) as single lines. Those candidate lines with obvious substructure in our lab spectra but no published hyperfine constants are dropped from further consideration.

In the end, we analyze 66 Co I lines in the HD 84937 spectrum. The abundances for all of these lines are given in Table 5. The last column of this table notes whether hyperfine substructure was taken into account (60 lines) or not (6 lines). We derive a mean abundance from all Co I lines of $\langle \log \varepsilon(\mathrm{Co}) \rangle = 2.785 \pm 0.008$ ($\sigma = 0.065$). The mean abundance from just the six lines analyzed without hyperfine substructure is 2.78, essentially identical to the overall mean. The line abundances are plotted as a function of wavelength in Figure 5. We do not find significant abundance trends with wavelength, excitation energy, transition probability, or line strength.

6. THE COBALT ABUNDANCE OF METAL-POOR STAR HD 84937 FROM IONIZED-SPECIES TRANSITIONS

Cobalt is almost completely ionized in the atmosphere of HD 84937, so it is not surprising that Co II absorption features can be detected in its UV spectrum. Moore et al. (1966) identify 23 lines of this species in the solar spectrum, all with $\lambda \leqslant 4660$ Å. Most of these transitions become undetectably weak in HD 84937, but other, stronger features become visible in the UV. Unfortunately, laboratory data for Co II are not extensive at present, thus some promising lines in HD 84937 cannot yield trustworthy abundances because reliable transition probabilities and/or hyperfine substructures are not available.

The NIST ASD lists no transition probability reference more recent than 1998. They assign highest weight to the laboratory results of Salih et al. (1985). We limit our search for Co II lines to those lines. Additionally, although Bergemann et al. (2010) have published hyperfine constants for some Co II levels, some

Table 5
Cobalt Abundances from Co I Lines in HD 84937

λ (Å)	χ (eV)	log(*gf*)	log ε	HFS?
2295.233	0.000	−0.80	2.77	yes
2323.145	0.101	−0.42	2.70	yes
2336.006	0.174	−0.54	2.87	yes
2338.665	0.224	−0.52	2.77	no
2352.869	0.431	−0.57	2.77	yes
2358.185	0.224	−1.09	2.67	yes
2380.490	0.101	−0.50	2.82	no
2407.255	0.000	0.71	2.72	yes
2411.624	0.101	0.60	2.82	yes
2414.463	0.174	0.47	2.64	yes
2424.935	0.000	0.52	2.72	yes
2439.040	0.224	0.00	2.79	yes
2521.365	0.000	0.34	2.77	yes
2544.255	0.224	−0.26	2.67	yes
2567.346	0.174	−0.73	2.77	no
3044.004	0.000	−0.55	2.90	yes
3061.820	0.101	−0.77	2.87	yes
3334.148	0.431	−1.05	2.79	yes
3367.110	0.431	−1.13	2.77	yes
3385.220	0.513	−1.03	2.84	yes
3388.168	0.581	−0.85	2.67	yes
3395.373	0.581	−0.49	2.79	yes
3405.118	0.431	0.29	2.73	yes
3409.176	0.513	−0.22	2.77	yes
3412.336	0.513	0.06	2.77	yes
3412.633	0.000	−0.71	2.92	yes
3417.157	0.581	−0.50	2.77	yes
3431.582	0.101	−0.90	2.87	yes
3433.039	0.629	−0.18	2.75	yes
3442.926	0.174	−1.05	2.82	yes
3443.645	0.513	−0.01	2.72	yes
3449.169	0.581	−0.12	2.75	yes
3449.440	0.431	−0.48	2.77	yes
3453.510	0.431	0.45	2.72	yes
3455.236	0.224	−1.19	2.87	yes
3462.805	0.629	−0.05	2.69	yes
3483.410	0.513	−1.01	2.74	no
3489.400	0.922	0.18	2.71	yes
3491.318	0.224	−1.41	2.86	yes
3495.682	0.629	−0.29	2.79	no
3502.280	0.431	0.11	2.77	yes
3506.313	0.513	0.02	2.74	yes
3512.640	0.581	−0.15	2.75	yes
3513.480	0.101	−0.79	2.87	yes
3518.348	1.048	0.00	2.73	yes
3521.566	0.431	−0.74	2.80	yes
3526.850	0.000	−0.59	2.89	yes
3529.033	0.174	−0.89	2.89	yes
3533.358	0.224	−1.03	2.87	yes
3550.594	0.174	−1.59	2.84	yes
3560.893	0.629	−0.82	2.84	yes
3564.951	0.581	−0.96	2.84	yes
3569.376	0.922	0.34	2.71	yes
3574.965	0.581	−0.77	2.87	yes
3627.807	0.513	−1.06	2.85	yes
3842.049	0.922	−0.74	2.77	yes
3845.468	0.922	0.06	2.77	yes
3873.114	0.431	−0.57	2.82	yes
3873.955	0.513	−0.81	2.84	yes
3881.874	0.581	−1.09	2.80	yes
3894.077	1.048	0.12	2.67	yes
3935.969	0.922	−0.86	2.77	no
3995.307	0.922	−0.18	2.77	yes
3997.903	1.048	−0.87	2.82	yes
4118.773	1.048	−0.48	2.80	yes
4121.318	0.922	−0.33	2.83	yes

Table 5
(Continued)

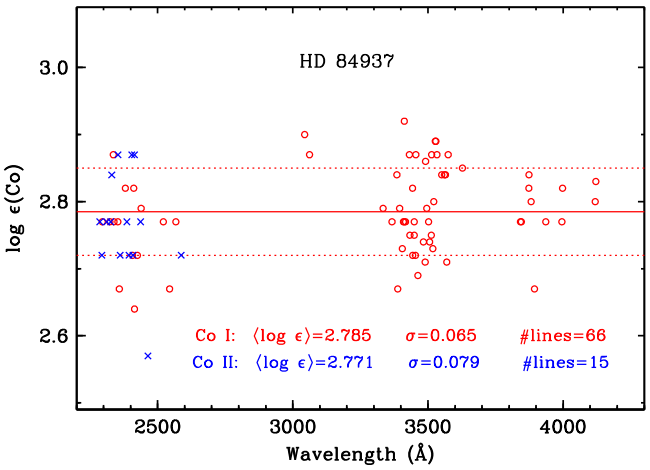

Figure 5. Cobalt abundances in HD 84937 from Co I lines (red circles) and Co II lines (blue × symbols) plotted as a function of wavelength. The abundance statistics for both species are given in the figure legend. The solid red line indicates the mean abundance derived from Co I lines, and the dotted red lines 1σ deviations from the mean.

of their results are only upper limits and the uncertainties in others are large. It is clear that a comprehensive attack on this ion cannot be attempted until further lab studies are undertaken. However, it is important to try to derive a Co abundance with the available data in order to understand whether a large difference with the result from Co I is suggested. This will indicate whether significant NLTE effects are present in the ionization equilibrium between the two Co species.

Our approach begins with limiting the potential Co II lines to only those estimated to be reliable in the NIST ASD, almost all of which are from Salih et al. (1985). The line at 2404 Å from Salih et al., but omitted from the NIST ASD, is added. The three additional longest wavelength lines in Table 6 are added from Mullman et al. (1998). Four more lines at 2326, 2361, 2386, and 2408 Å are added in this study using the new accurate Ritz wave numbers (Pickering et al. 1998) to resolve blending problems listed in Table 1 of Salih et al. (1985). Resolution of those blends yields branching fractions for lines from the z^5F_2 and z^5D_2 levels which we combine with lifetimes in Salih et al. (1985). Additional work on Co II is underway. We identify nearly 20 transitions, but using preliminary synthetic spectrum calculations we prune them to a set of 16 that are sufficiently unblended for abundance analysis. Then we construct approximate hyperfine substructures for the single naturally occurring isotope ^{59}Co, which has a nuclear spin $I = 7/2$. For each line, we find the number of hyperfine components and their relative intensities from the lower and upper level J using Table 1 of Chapter IX in "*The Theory of*

Table 6
Cobalt Abundances from Co II Lines in HD 84937

λ (Å)	χ (eV)	log(*gf*)	logϵ	HFS?
2286.159	0.415	0.53	2.77	yes
2293.389	0.565	−0.74	2.72	no
2311.604	0.565	0.31	2.77	no
2326.135	0.565	−0.46	2.77	yes
2330.357	0.613	−0.49	2.84	no
2353.422	0.565	0.04	2.87	yes
2361.520	0.645	−1.12	2.82	no
2386.368	0.565	−0.04	2.77	yes
2393.904	0.565	−1.11	2.72	yes
2404.172	0.645	−0.41	2.87	no
2408.753	0.613	−0.38	2.72	no
2414.069	0.565	−0.36	2.87	yes
2436.979	0.613	−1.06	2.77	yes
2464.199	1.216	−0.42	2.57	yes
2580.326	1.216	0.36	2.47	yes
2587.219	1.327	0.03	2.72	no

Atomic Spectra" by Condon & Shortley (1951).[9] Relative intensities from the table are then normalized to sum to 1.0. Finally component *gf* values are calculated from the total line *gf* and these normalized intensities. An upper or lower level hfs *A* coefficient must then be estimated so that the component pattern matches the observed line width using the standard hfs component shift expression (e.g., Woodgate 1980). Magnetic dipole hfs *A* coeffficients are almost always dominant and electric quadrupole hfs *B* coefficients are very rarely needed in stellar spectroscopy. The resulting hyperfine components are used in synthetic spectrum calculations to derive an abundance from the Co II feature. Our approximate hyperfine patterns are good enough to mimic the true desaturation of Co II lines, but are no substitute for determination of good hyperfine constants from laboratory spectra. Further work in this area will be welcome.

From the 16 Co II line abundances (Table 6) the mean abundance is $\langle \log \varepsilon(\mathrm{Co\ II}) \rangle = 2.753 \pm 0.027$ ($\sigma = 0.107$), a value that is essentially identical to that determined from Co I lines for HD 84937. We illustrate the general consistency of Co I & II line abundances in Figure 6. The abundances derived from the Co II line at 2639.97 Å and the Co I line at 2639.04 Å are very similar.

Bergemann et al. (2010) included one Co II line in their study of NLTE effects on Co abundances. This line occurs at 3501.7 Å and arises from a level with excitation energy $\chi = 2.20$ eV. Bergemann et al. adopted a theoretical transition probability from Raassen et al. (1998): $\log(gf) = -1.22$ (the value in the NIST database is −0.94). We attempt to derive an abundance from this line also. It is detectable in our UVES spectrum of HD 84937, but its maximum depth is only about 3%, not much larger than the typical ±1% continuum noise fluctuations. We derive $\log \varepsilon \approx 2.8$, consistent with the mean of the stronger Co II lines. From our analysis we cannot detect an ionization imbalance in the two Co species.

[9] Although the table is described in terms of line strengths for Russell–Saunders multiplets, it is applicable to hfs coupling problems. Woodgate (1980) explains that hfs coupling $F = J + I$ is analogous to perfect Russell–Saunders coupling in which $J = L + S$.

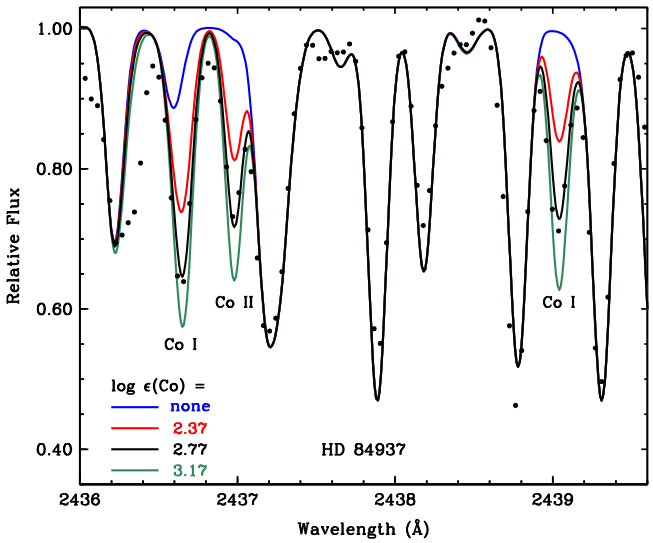

Figure 6. Comparison of synthetic and observed spectra in a small UV wavelength interval of HD 84937. This region has been chosen to contain lines of both Co species. The observed spectrum is shown as filled circles, and the syntheses are shown as colored lines representing abundances that are given in the figure caption. The Co abundance labeled "none" means that this synthetic spectrum was computed without any Co contribution. Note that we do not include the Co I line at 2436.6 Å in our abundance calculations, as it is deemed to be too blended.

7. THE RELATIVE ABUNDANCE OF COBALT AND IRON IN HD 84937

Sneden et al. (2015) derive $\log \varepsilon(\mathrm{Fe\ I})_{\mathrm{Sun}} = 7.522 \pm 0.004$ ($\sigma = 0.05$) and $\log \varepsilon(\mathrm{Fe\ II})_{\mathrm{Sun}} = 7.511 \pm 0.021$ ($\sigma = 0.08$), and 5.202 ± 0.003 ($\sigma = 0.07$) and 5.191 ± 0.005 ($\sigma = 0.06$), respectively, for HD 84937. With these values, we find $[\mathrm{Fe\ I/H}] = -2.32$ and $[\mathrm{Fe\ II/H}] = -2.32$, in excellent agreement with each other. For Co, combining the solar abundance of $\log \varepsilon = 4.955 \pm 0.007$ ($\sigma = 0.059$) with the HD 84937 value of 2.785 ± 0.008 ($\sigma = 0.065$) yields $[\mathrm{Co\ I/H}] = -2.17$. Since we do not determine a Co abundance from Co II in the Sun, we assume our derived solar value from Co I, so $\log \varepsilon(\mathrm{Co\ II}) = 2.753 \pm 0.027$ ($\sigma = 0.107$), leads to $[\mathrm{Co\ II/H}] = -2.19$. These abundances in turn yield $[\mathrm{Co/Fe}] = +0.15$ for Co I and +0.13 for Co II. Thus, we do not see any obvious violation of LTE in the ionization equilibrium of Co.

Bergemann et al. (2010) report that $[\mathrm{Co/Fe}] = +0.18$ assuming LTE, which is in excellent agreement with our result. But they also suggest that the NLTE abundance ratio is +0.66, nearly 0.5 dex larger. They further find that the NLTE correction for Co I is ∼+0.6, while that for Co II is ∼+0.1. This result appears to be incompatible with our results, which are admittedly derived from a traditional LTE abundance analysis. Further study of Co line formation in metal-poor stellar atmospheres would be welcome.

The abundance of this element, along with the other iron-peak elements, is critical to our understanding of supernova nucleosynthesis, particularly at low metallicities, and Galactic chemical evolution (gce). Our newly derived (average) value of $[\mathrm{Co/Fe}] = 0.14$ for HD 84937 is compatible with other observations of this element in stars of similar metallicity (see the recent compilation of Roederer et al. 2014). Further, the slight overabundance of Co found for HD 84937 at $[\mathrm{Fe/H}] = -2.3$ is in accord with the general rising trend at

Table 7
Hyperfine Structure (hfs) Line Component Patterns for 195 Transitions of ^{59}Co I Computed from Published hfs Coefficients (See Text), Energy Levels of Pickering & Thorne (1996), and the Standard Index of Air (Peck & Reeder 1972)

Transition Wavenumber (cm^{-1})	Wavelength in Air (Å)	F_{upp}	F_{low}	Component Position (cm^{-1})	Component Position (Å)	Strength Normalized to 1.0 for Each Transition
43555.148	2295.2326	7	8	0.05135	−0.002706	0.21250
43555.148	2295.2326	7	7	0.17328	−0.009132	0.02083
43555.148	2295.2326	7	6	0.27900	−0.014704	0.00104
43555.148	2295.2326	6	7	0.00952	−0.000502	0.16667
43555.148	2295.2326	6	6	0.11524	−0.006073	0.03385

Note. Center-of-gravity wavenumbers and air wavelengths are given with component positions relative to those values.

(This table is available in its entirety in machine-readable form.)

lower metallicities, as noted in other papers (see, e.g., Henry et al. 2010). Critical comparisons of Co to other iron-peak elements, particularly Cr, will be necessary to determine the nature of the early Galactic nucleosynthesis and gce (Sneden et al. 2015).

8. SUMMARY

New emission branching fractions from FTS and echelle spectrometer data are used in combination with radiative lifetimes from LIF measurements (Nitz et al. 1995) to determine accurate, absolute atomic transition probabilities for 898 lines of Co I. Complete hfs line component patterns for 195 lines of Co I found useful in abundance studies are determined from the best published hfs A and B coefficients. Applications of these new data yield Co abundance values in the Sun and metal-poor star HD 84937 of $\log \varepsilon(\mathrm{Co}) = 4.955 \pm 0.007$ ($\sigma = 0.059$) based on 82 Co I lines and $\log \varepsilon(\mathrm{Co}) = 2.785 \pm 0.008$ ($\sigma = 0.065$) based on 66 Co I lines, respectively, both using the Holweger-Müller 1D model. A similar analysis on HD 84937 using 16 Co II lines yields $\log \varepsilon(\mathrm{Co\ II}) = 2.753 \pm 0.027$ ($\sigma = 0.107$). The resulting value of $[\mathrm{Co/Fe}] = +0.14 \pm 0.03$ supports a rise of Co/Fe at low metallicity.

This work is supported in part by NASA grant NNX10AN93G (J.E.L.), by NSF grant AST-1211055 (J.E.L.), and NSF grant AST-1211585 (C.S.). The authors thank Michael Wood and Thomas Feigenson for assistance with echelle data.

APPENDIX

Cobalt has a single stable isotope ^{59}Co with a nuclear spin $I = 7/2$. Reliable abundance determinations on many lines require hfs component patterns. Fortunately much of the needed hfs data is available for Co I. Very little is available for Co II. Childs & Goodman (1968) measured hfs A and B coefficients using a radio frequency (RF) technique for the ground and six low metastable levels of neutral Co. Their hfs A coefficients have total uncertainties ∼1 kHz. Uncertainties on their hfs C coefficients typically overlapped zero and C coefficients are neglected here. Guthöhrlein & Keller (1990) measured hfs A and B coefficients using a Doppler-free laser spectroscopy technique for additional even parity metastable levels and some odd parity levels. Their hfs A coefficients have total uncertainties ∼1 MHz. Additional small sets of measurements were reported by:Behrens et al. (1994), Clüa-Gonzalez (1990), Ibrahim-Rüd (1985), Ortel (1970), Rasmussen (1936), and Wenzel (1987). Pickering (1996) used line profile fitting on FTS spectra to measure hfs A and B coefficients for 297 levels. Her new results are compared to the smaller sets of earlier measurements in her publication. Pickering's hfs data are of similar quality or better quality than the smaller sets of earlier measurements except for the above mentioned RF and Doppler-free laser spectroscopy measurements. We used the clearly superior RF (Childs & Goodman 1968) and Doppler-free (Guthöhrlein & Keller 1990) hfs coefficients where available and adopted Pickering's hfs coefficients for all other levels to determine the complete hfs component patterns for 195 lines of Co I in Table 7. A final check was performed during the preparation of Table 7. Each computed hfs component pattern for a line of Co I was compared to our best FTS line profile for that line.

REFERENCES

Adams, D. L., & Whaling, W. 1981, JOSA, 71, 1036
Asplund, M. 2005, ARA&A, 43, 481
Behrens, H. O., Dembczynski, J., Farber, M., et al. 1994, ApPhB, 59, 299
Bergemann, M., Pickering, J. C., & Gehren, T. 2010, MNRAS, 401, 1334
Brault, J. W. 1976, JOSA, 66, 1081
Bridges, J. M., & Ott, W. R. 1977, ApOpt, 16, 367
Cardon, B. L., Smith, P. L., Scalo, J. M., Testerman, L., & Whaling, W. 1982, ApJ, 260, 395
Childs, W. J., & Goodman, L. S. 1968, PhRv, 170, 50
Clüa-Gonzalez, A. L. 1990, JOSA, 68, 251
Condon, E. U., & Shortley, G. H. 1951, The Theory of Atomic Spectra (Cambridge: Cambridge Univ. Press)
Danzmann, K., & Kock, M. 1982, JOSA, 72, 1556
Delbouille, L., Roland, G., & Neven, L. 1973, Photometric Atlas of the Solar Spectrum from λ3000 to λ10000 (Liège: Inst. daAp. Univ. de Liège)
Den Hartog, E. A., Lawler, J. E., Sobeck, J. S., Sneden, C., & Cowan, J. J. 2011, ApJS, 194, 35
Den Hartog, E. A., Ruffoni, M. P., Lawler, J. E., et al. 2014, ApJS, 215, 23
Figger, H., Heldt, J., Siomos, K., & Walther, H. 1975, A&A, 43, 389
Fulbright, J. P. 2000, AJ, 120, 1841
Gratton, R. G., Carretta, E., Claudi, R., Lucatello, S., & Barbieri, M. 2003, A&A, 404, 187
Guthöhrlein, G. H., & Keller, H. P. 1990, ZPhyD, 17, 181
Hashiguchi, S., & Hasikuni, M. 1985, JPSJ, 54, 1290
Henry, R. B. C., Cowan, J. J., & Sobeck, J. 2010, ApJ, 709, 715
Holweger, H., & Müller, E. A. 1974, SoPh, 39, 19
Ibrahim-Rüd, J. 1985, Diplomarbeit (Hamburg: Univ. Bundeswehr)
Kramida, A., Ralchenko, Yu., Reader, J. & NIST ASD Team 2014, NIST Atomic Spectra Database (ver. 5.1) [Online]. Available: http://physics.nist.gov/asd [2015, May 19]. National Institute of Standards and Technology, Gaithersburg, MD
Lawler, J. E., Bilty, K. A., & Den Hartog, E. A. 2011, J. Phys. B:At. Mol. Opt. Phys., 44, 095001
Lawler, J. E., Guzman, A., Wood, M. P., Sneden, C., & Cowan, J. J. 2013, ApJS, 205, 11
Lawler, J. E., Wood, M. P., Den Hartog, E. A., et al. 2014, ApJS, 215, 20

Lodders, K., Palme, H., & Gail, H.-P. 2009, Landolt-Börnstein—Group VI Astronomy and Astrophysics, Vol. 4B (Berlin: Springer)
Marek, J., & Vogt, K. 1977, ZPhyA, 280, 235
McWilliam, A. 1997, ARA&A, 35, 503
Moore, C. E., Minnaert, M. G. J., & Houtgast, J. 1966, The Solar Spectrum 2935 Å to 8770 Å, Vol. 61 (Washington, DC: GPO)
Mullman, K. L., Cooper, J. C., & Lawler, J. E. 1998, ApJ, 495, 503
Nitz, D. E., Bergeson, S. D., & Lawler, J. E. 1995, JOSAB, 12, 377
Nitz, D. E., Kunau, A. E., Wilson, K. L., & Lentz, L. R. 1999, ApJS, 122, 557
Ortel, K. B. 1970, ZPhy, 236, 90
Peck, E. R., & Reeder, K. 1972, JOSA, 62, 958
Pickering, J. C. 1996, ApJS, 107, 811
Pickering, J. C., Raassen, A. J. J., Uylings, P. H. M., & Johansson, S. 1998, ApJS, 117, 261
Pickering, J. C., & Thorne, A. P. 1996, ApJS, 107, 761
Raassen, A. J. J., Pickering, J. C., & Uylings, P. H. M. 1998, A&AS, 130, 541
Rasmussen, E. 1936, ZPhy, 102, 229
Roederer, I. U., Preston, G. W., Thompson, I. B., et al. 2014, AJ, 147, 136
Ruffoni, M. P., Den Hartog, E. A., Lawler, J. E., et al. 2014, MNRAS, 441, 3127
Salih, S., Lawler, J. E., & Whaling, W. 1985, PhRvA, 31, 744
Scott, P., Asplund, M., Grevesse, N., Bergemann, M., & Jacques Sauval, A. 2015, A&A, 573, A26
Sneden, C. 1973, ApJ, 184, 839
Sneden, C., Cowan, J. J., Kobayashi, C., et al. 2015, ApJ, submitted
Sobeck, J. S., Kraft, R. P., Sneden, C., et al. 2011, AJ, 41, 175
Sobeck, J. S., Lawler, J. E., & Sneden, C. 2007, ApJ, 667, 1267
Wenzel, R. 1987, Diplomarbeit (Hamburg: Univ. Bundeswehr)
Whaling, W., Carle, M. T., & Pitt, M. L. 1993, JQSRT, 50, 7
Wickliffe, M. E., Lawler, J. E., & Nave, G. 2000, JQSRT, 66, 363
Wood, M. P., & Lawler, J. E. 2012, ApOpt, 51, 8407
Wood, M. P., Lawler, J. E., Den Hartog, E. A., Sneden, C., & Cowan, J. J. 2014a, ApJS, 214, 18
Wood, M. P., Lawler, J. E., Sneden, C., & Cowan, J. J. 2013, ApJS, 208, 27
Wood, M. P., Lawler, J. E., Sneden, C., & Cowan, J. J. 2014b, ApJS, 211, 20
Woodgate, G. K. 1980, Elementary Atomic Structure (2nd ed.; Oxford: Clarendon)